Optimal design of detector thickness for dual-energy x-ray imaging

Dong Woon Kim [a], Ho Kyung Kim [a,b*]
[a] School of Mechanical Engineering, Pusan National University, Busan, South Korea
[b] Center for Advanced Medical Engineering Research, Pusan National University, Busan, South Korea
[*] Corresponding author: hokyung@pusan.ac.kr

1. Introduction

The projection of three-dimensional (3D) human body on a two-dimensional (2D) radiograph results in the superimposition of normal tissue that can obscure abnormalities and in some common cases be misread as abnormalities[1]. To reduce or eliminate this effect, 3D depth-discrimination techniques such as computed tomography can be used[2]. Another method for improving conspicuity of abnormalities is an energy-discrimination technique such as dual-energy imaging (DEI). The DEI discriminates, or enhances, material content (e.g. bone or soft tissue) within a 2D radiograph by combining images obtained at separte low and high energies[3].

A commercial DEI system uses the fast kilovoltage (kVp) switching technique, which acquires low and high-kVp projections in successive x-ray exposure[4, 5]. To obtain better quality in DE images, a large energy separation between the low and high-kVp setups is typically used for chest (e.g. 60/120 kVp). While it is typically known that the detector performance is dependent on which x-ray converter is used and which energy is used for imaging[6], and there exists an optimal thickness of x-ray converter (e.g. cesium iodide, CsI) with respect to energies used for imaging[7], the DEI uses the same detector for acquiring two different projections for the low and high-kVp setups.

In this study, we theoretically investigate the effect of different thicknesses of CsI on soft tissue-enhanced DE images. Detectability index is accounted for evaluating the DEI performance with respect to various combinations of CsI thicknesses used for each low and high kVp. The noise-power spectrum (NPS) or noise-equivalent number of quanta (NEQ) is determined from the cascaded-systems analysis (CSA) with published detector parameters.

2. Theoretical background

2.1 Detectability index
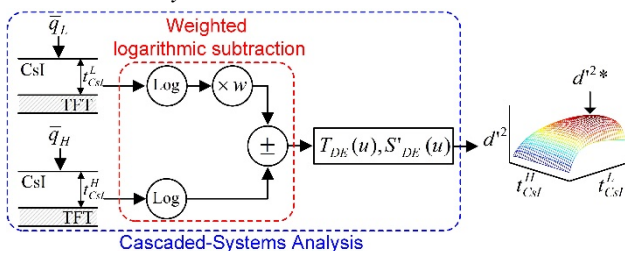
Fig. 1. Schematic illustration of the optimization strategy to determine the CsI thickness for given dual-energy imaging simulations

Detectability index for the prewhitening (PW) matched filter observer model is given by[8]

$$(d'_{PW})^2 = \int \int \frac{\{T(u,v)W(u,v)\}^2}{S'(u,v)} \mathrm{d}u\mathrm{d}v, \qquad (1)$$

where $W(u,v)$ denotes a task function. $T(u,v)$ and $S'(u,v)$ denotes the MTF and normalized NPS (NNPS), respectively, in the (u,v) frequency coordinates. There two metrics are related to the NEQ:

$$\mathrm{NEQ}(u,v) = \frac{T^2(u,v)}{S'(u,v)}. \qquad (2)$$

The index described above can be extended to include a human eye filter $E(u,v)$ and internal noise N_{int}: [8, 9]

$$(d'_{PWE})^2 = \int \int \frac{E^2(u,v)\{T(u,v)W(u,v)\}^2}{E^2(u,v)S'(u,v) + N_{int}} \mathrm{d}u\mathrm{d}v. \qquad (3)$$

2.2 Dual-energy Fourier metrics

The detective quantum efficiency (DQE) in DE images may be expressed in the conventional DQE form:

$$\mathrm{DQE}_{DE}(u,v) = \frac{T_{DE}^2(u,v)}{S'_{DE}(u,v)\overline{q}_{DE}}, \qquad (4)$$

where $\overline{q}_{DE}$ denotes the incident photon fluence used for DEI. Assuming that the DE images are obtained from the weighted logarithmic subtraction of two images obtained for low and high kVp's and the two images are independent to each other, $S'_{DE}(u,v)$ is the given by

$$S'_{DE}(u,v) = w^2 S'_L(u,v) + S'_H(u,v), \qquad (5)$$

where w is the weighting factor for enhancing soft tissue in DE images, and the subscripts L and H represent low and high-kVp images, respectively.

Combining the DE deterministic NNPS defined by Richard *et al.*[10] and Eq. (4), $T_{DE}(u,v)$ may be given by

$$T_{DE}(u,v) = \left[w^2 \frac{\overline{q}_{DE}}{\overline{q}_L} T_L^2(u,v) + \frac{\overline{q}_{DE}}{\overline{q}_H} T_H^2(u,v) \right]^{1/2}. \qquad (6)$$
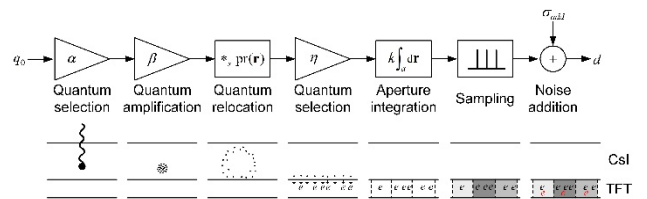
Fig. 2. Cascaded linear-systems model to describe signal and noise propagation in hypothetical CsI-based detectors

3. Methods

In this theoretical work, hypothetical flat-panel detectors (CsI-coupled to amorphous silicon photodiode panels) were considered. Various CsI thicknesses ranging 10-300 mg cm^{-2} were considered for imaging. The pixel pitch p and fill factor γ were assumed to be 0.15 mm and 75%, respectively. Additive electronic noise (σ_{add}) of detectors was assumed as 3×10^3 electrons.

From the cascaded linear-systems theory[11, 12], as described in Fig. 2, the NNPS can be given by

$$S'(u,v) = \frac{1}{\bar{q}_0}\left[\frac{1}{\gamma\bar{g}} + \frac{T'^2(u,v)}{\alpha}\left(\frac{1}{I} - \frac{1}{\beta}\right)\right] + \frac{p^2\sigma_{add}^2}{\bar{q}_0^2\bar{g}^2} \quad (7)$$

with

$$\bar{g} = ka^2\alpha\beta\eta \quad (8)$$

and

$$T'^2(u,v) = \sum_{i=0}^{\infty}\sum_{j=0}^{\infty} T^2\left(u\pm\frac{i}{p}, v\pm\frac{j}{p}\right), \quad (9)$$

where $\bar{q}_0$ = incident photon fluence, α = CsI quantum efficiency, β = the optical quantum gain per x-ray interaction, η = the photodiode quantum efficiency, a = the one-directional size of sensitive pixel with the square geometry of pixel, and k = the scaling factor to digital units at the pixel output. The detector output is given by $\bar{d} = \bar{q}_0\bar{g}$.

4. Preliminary results

Figure 3 summarizes CSA results of the hypothetical CsI detectors. The spatial resolution performances of CsI with various thicknesses are plotted in Fig. 3(a) in the form of the size of effective aperture: $a_{eff} = \left[2\pi\int_0^{\infty}T(f)fdf\right]^{-1}$. The a_{eff} was increased, due to larger probability in optical scattering, with increasing t_{CsI} . The noise relative to detector output signal was calculated from the square root of the integration of $S'(u,v)$, which was calculated using Eq. (7) for various t_{CsI} , within the extent of the Nyquist frequencies (i.e. $\sigma^2/\bar{d}^2 = \int_{-v_N}^{v_N}\int_{-u_N}^{u_N}S'(u,v)dudv$). The results are shown in Fig. 3(b). The DQE results at the frequencies
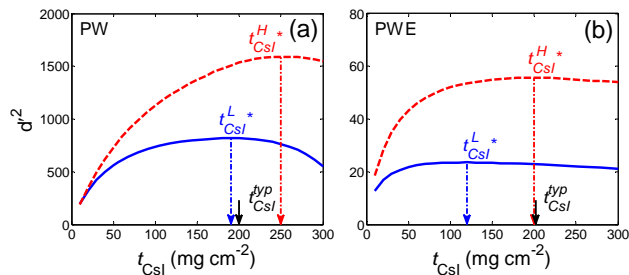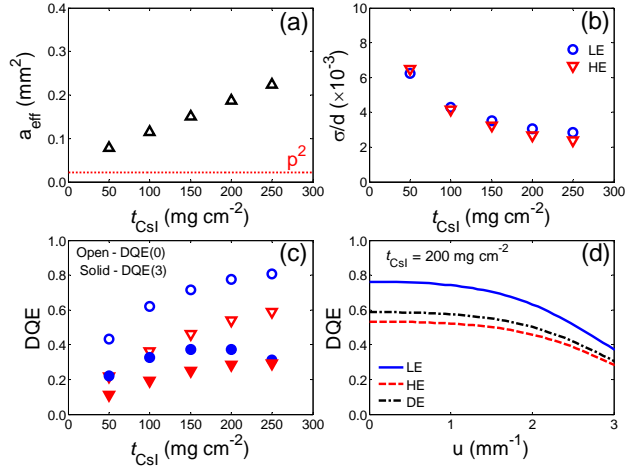
Fig. 3. Summary of hypothetical detector performances for various CsI thickness: (a) Effective aperture, (b) relative noise, (c) DQE at the frequencies of 0 and 3 mm^{-1}, and (d) the spatial-frequency-dependent DQEs of the detector with $t_{CsI} = 200$ mg cm^{-2} for low and high kVp's, and their resultant DE DQE.

of zero and 3 mm^{-1} as functions of t_{CsI} are shown in Fig. 3(c). The DQE(0) was increased with increasing t_{CsI} for both the low and high kVp's, and the simple formalism of DQE(0) $\approx \alpha I$ well described the results calculated by CSA. While the DQE(3) for the high-kVp spectrum was increased with increasing t_{CsI} and then saturated around t_{CsI} =~ 200 mg cm^{-2}, the DQE(3) for the low-kVp spectrum showed the maximum value around t_{CsI} =~ 170 mg cm^{-2} and the decreased. Figure 3(d) shows the DQE(u)'s of the hypothetical detector with t_{CsI} =~ 200 mg cm^{-2} for the two spectra and their resultant DE DQE(u) which is placed between the two DQE(u) results.

Detectability indexes calculated for conventional radiography for various CsI thicknesses are shown in Fig. 4. For the PW model, the typical CsI thickness was located between the optimal CsI thickness calculated for low and high-kVp spectra as shown in Fig. 4(a). On the other hand, the detectability indexes for the PWE model was less dependent on t_{CsI} compared to that for the PW model as shown in Fig. 4(b).

5. Discussion and Conclusion

The optimal CsI thickness for dual-energy chest imaging has been theoretically investigated by evaluating prewhitening observer model detectability indexes. To evaluate the PW and PWE detectability indexes, dual-energy fluence and MTF have reviewed compared to the conventional descriptions. From the calculation results for conventional radiography, the typical CsI thickness of 200 mg cm^{-2} was placed between low and high-energy CsI thickness.

Fig. 4. Detectability indexes calculated for conventional radiography for various CsI thicknesses: (a) PW and (b) PWE models.

REFERENCES

[1] H. Youn, J. C. Han, M. K. Cho, S. Y. Jang, H. K. Kim, J. H. Kim, J. Tanguay, and I. A. Cunningham, Numerical generation of digital mammograms considering imaging characteristics of an imager, Nucl. Instrum. Meth. A, Vol.652, pp.810-814, 2011.
[2] J. T. Dobbins, Tomosynthesis imaging: At a translational crossroads, Med. Phys., Vol.36, pp.1956-1967, 2009.
[3] N. A. Shkumat, J. H. Siewerdsen, A. C. Dhanantwari, D. B. Williams, S. Richard, N. S. Paul, J. Yorkston, and R. Van Metter, Optimization of image acquisition techniques for dual-energy imaging of the chest, Med. Phys. Vol.34, pp. 3904–3915, 2007.
[4] N. A. Shkumat, J. H. Siewerdsen, A. C. Dhanantwari, D. B. Williams, N. S. Paul, J. Yorkston, and R. V. Metter, Cardiac gating with a pulse oximeter for dual-energy imaging, Phys. Med. Biol., Vol. 53, pp. 6097–6112, 2008.
[5] H. Kashani, C. A. Varon, N. S. Paul, G. J. Gang, R. V. Metter, J. Yorkston, and J. H. Siewerdsen, Diagnostic performance of a prototype dual-energy chest imaging system: ROC analysis, Acad. Radiology, Vol.17, pp. 298–308, 2010.
[6] H. Jeon, M. J. Chung, S. Youn, J. Nam, J. Lee, D. Park, W. Kim, Y. Ki, and H. K. Kim, Imaging responses of on-site CsI and Gd2O2S flat-panel detectors: Dependence on the tube voltage, J. Korean Phys. Soc., Vol.67, pp. 264–269, 2015.
[7] J. H. Siewerdsen, and L. E. Antonuk, DQE and system optimization for indirect-detection flat-panel imagers in diagnostic radiography, Proc. SPIE, Vol.3336, pp.546–556, 1998.
[8] A. E. Burgess, X. Li, and C. K. Abbey, Visual signal detectability with two noise components: Anomalous masking effects, J. Opt. Soc. Am. A., Vol.14, pp. 2420–2442, 1997.
[9] G. J. Gang, J. Lee, J. W. Stayman, D. J. Tward, W. Zbijewski, J. L. Prince, and J. H. Siewerdsen, Analysis of fourier-domain task-based detectability index in tomosynthesis and cone-beam CT in relation to human observer performance, Med. Phys., Vol.38, pp. 1754–1768, 2011.
[10] S. Richard, J. H. Siewerdsen, D. A. Jaffray, D. J. Moseley, and B. Bakhtiar, Generalized DQE analysis of radiographic and dual-energy imaging using flat-panel detectors, Med. Phys., Vol.32, pp. 1397–1413, 2005.
[11] S. Yun, C. H. Lim, H. K. Kim, J. Tanguay, and I. A. Cunningham, Finding the best photoconductor for digital mammography detectors, Nucl. Instrum. Meth. A, Vol.652, pp. 829–833, 2011.
[12] H. K. Kim, C. H. Lim, J. Tanguay, S. Yun, and I. A. Cunningham, Spectral analysis of fundamental signal and noise performances in photoconductors for mammography, Med. Phys., Vol.39, pp. 2478–2490, 2012.